CrystEngComm

Accepted Manuscript

ROYAL SOCIETY OF CHEMISTRY

www.rsc.org/crystengcomm

Cite this: DOI: 10.1039/c0xx00000x

www.rsc.org/xxxxxx

ARTICLE TYPE

Hydrothermal synthesis and formation mechanism of photocatalytically active $SrTiO_3$ nanocrystals using anatase TiO_2 with different facets as a precursor

Jingmiao Peng[a],[b], Ying Zhou*[a],[b], Hao Wang[c], Haoran Zhou[b], Shiyi Cai[b]

Received (in XXX, XXX) Xth XXXXXXXXX 20XX, Accepted Xth XXXXXXXXX 20XX
DOI: 10.1039/b000000x

Strontium titanate ($SrTiO_3$) nanocrystals have been synthesized by a hydrothermal reaction route using anatase TiO_2 nanosheets with dominant {001} facets and commercial anatase TiO_2 nanoparticles as precursors. Time resolved quenching experiments showed the velocity of hydrothermal formation of $SrTiO_3$ was relatively fast (in minutes). The initial particle morphology and exposed crystal facets of anatase TiO_2 precursor cannot be retained in the final $SrTiO_3$ products. $SrTiO_3$ nuclei is formed by the reaction between $Ti(OH)_x^{4-x}$ and Sr ions at the TiO_2 solid/liquid interface. As surface adsorbed F^- is necessary to stabilize the {001} facets of anatase TiO_2, the hydrothermal crystallization of $SrTiO_3$ from TiO_2 with {001} facets not only exhibits a slower reaction rate but also a higher activation energy. Moreover, the photoelectrochemical and photocatalytic activity studies indicated that the $SrTiO_3$ products obtained from TiO_2 with {001} facets showed enhanced photocurrent density and photocatalytic hydrogen production activity. The present study sheds some light on the understanding of the crystal facets of precursor on the hydrothermal formation process as well as their photocatalytic activities of the corresponding products.

1 Introduction

Strontium titanate ($SrTiO_3$) is a typical representative of the family of perovskite-type oxides (ABO_3), which have wide applications in oxygen gas sensor, photocatalysts, storage batteries and photoelectrodes for dye-sensitized solar cell, etc.[1-4] It is generally accepted that the application performances of materials are strongly related to their size, morphology, defects and surface properties, which on the other hand depend on the preparation methods and conditions.[5] Traditionally, $SrTiO_3$ are synthesized by solid-state-reaction of strontium carbonate and titanium dioxide with temperature typically higher than 900℃.[6] Later on, hydrothermal method has been reported as a mild approach to synthesize of $SrTiO_3$ with temperature below 200℃.[7] Since then, intense efforts have been focused on the size and morphology modification of $SrTiO_3$ by hydrothermal method. Some groups have prepared $SrTiO_3$ via an one-step hydrothermal method through the use of organic and inorganic additives as a tool of morphology control and structure-directing template. For example, $SrTiO_3$ nanoparticles were obtained by adjusting the concentration of KOH and silicate.[8, 9] Oriented aggregate $SrTiO_3$ were formed by the aid of organic additives.[10-13] Alteration of the additives has a significant effect on the morphology and characteristics of the final products, and thus the corresponding properties can be tuned by varying time, additives and some other preparation parameters.

Compared to the use of liquid Ti precursor, solid TiO_2 with different morphology were prepared in advance and then they react with Sr precursor and simultaneously play a role as template. Consequently, the final product could retain the morphology of the solid precursor, which brings a new insight on the use of self-template approaches to prepare nanofibers,[14-16] nanotubes[17-19] and porous $SrTiO_3$.[20, 21] In addition to the advantage of morphology control, through adjusting the preparation parameters, $SrTiO_3/TiO_2$ nanocomposite can be fabricated by this strategy as well.[9] Due to the well matching of the position of the conduction band (CB) and valence band (VB) between $SrTiO_3$ and TiO_2, $SrTiO_3/TiO_2$ nanocomposite exhibited improved charge transfer and separation efficiency as well as enhanced photocatalytic activity.[15] Although in situ X-ray diffraction (XRD) technique has been performed to understand the hydrothermal crystallization of $BaTiO_3$[22] and $CaTiO_3$[23] using TiO_2 as a precursor and two extreme models have been proposed: the dissolution-precipitation mechanism and in situ heterogeneous transformation mechanisms,[22] little is known about the hydrothermal formation mechanism of $SrTiO_3$.

Moreover, the crystal structure of TiO_2 precursor could have significant influence on the hydrothermal crystallization of $SrTiO_3$. Kutty et al. demonstrated that amorphous TiO_2 gels reacted fastest, rutile TiO_2 reacted most slowly, and antase phase exhibited intermediate kinetics.[24] Recently, the pioneer work from Yang et al. indicated that anatase TiO_2 with {001} facets whose surface energy (0.90 J/m^2) is much higher than that of thermodynamically stable {101} facets (0.44 J/m^2) can be

stabilized by F^-.[25] They further investigated the hydrothermal stability of {001} faceted anatase TiO_2, which tend to eliminate steadily along [001] crystallographic direction.[26] Contrarily, anatase TiO_2 with dominant {101} facets is highly stable under hydrothermal condition.[26] Therefore, it can be expected that even the TiO_2 precursor with the same crystal structure but with different exposing crystal facets could have different chemical reactivity and thus affect the hydrothermal crystallization of $SrTiO_3$. Unfortunately, the role of crystal facets of TiO_2 precursor on the hydrothermal formation mechanisms of $SrTiO_3$ has never been reported up to now. In addition, it is also unclear whether the precursor dominated by different crystal facets could promote the formation of $SrTiO_3$ with different facets or not.

In the following, we investigate the hydrothermal crystallization of $SrTiO_3$ using anatase TiO_2 nanosheets with dominant {001} facets and commercial anatase TiO_2 nanoparticles as precursors by time resolved quenching experiments. Moreover, the photoelectrochemical (PEC) properties and photocatalytic hydrogen production activities of $SrTiO_3$ products obtained from different TiO_2 precursors are compared.

2 Experiment

2.1 Anatase TiO_2 precursors with different crystal facets

The synthesis of TiO_2 nanosheets with exposed {001} facets (denoted as "TO-NS" below) was carried out via a hydrothermal route using tetrabutyl titanate [$Ti(OC_4H_9)_4$] as Ti source and hydrofluoric acid (HF) solution as solvent, according to previously reported method.[27] *Caution! Hydrofluoric acid is extremely corrosive and a contact poison, and it should be handled with extreme care*. In a typical procedure, 3.75 mL $Ti(OC_4H_9)_4$ was placed into a dried Teflon-lined stainless steel autoclave with a capacity of 15 mL. Then 0.6 mL of HF solution was dropped into the above liquid slowly. The mixture was heated to 200 °C and kept for 24 h in oven. After reaction, the products were neutralized and washed with deionized water and ethanol for several times, and dried at 50 °C for 24 h. The anatase TiO_2 nanoparticles (denoated as "TO-NP", 99.8%) were ordered from Aladdin Chemistry Co. Ltd. All chemicals were used without any further treatment.

2.2 Synthesis of $SrTiO_3$ nanocrystals and quenching experiments

Both TO-NP and TO-NS were used as Ti precursors. In a typical procedure, 2.5 mmol Ti precursor and 2.5 mmol $Sr(OH)_2$ were dissolved in 15 mL deionized water in a Teflon-lined stainless steel autoclave with a capacity of 40 mL, the pH of the suspension was adjusted to be higher than 13 using 8 M KOH. The mixture was heated to 160 °C and kept for 24h in oven. After reaction, the products were filtered and washed with deionized water and ethanol for several times, and dried at 50 °C for 24 h.

In order to investigate the crystallization process of the products from different Ti precursors, the reaction was performed by rapid cooling experiment using Duran quartz glass tubes. The tube was acted as an autoclave to produce high temperature and pressure, 0.25 mmol Ti precursor and 0.25 mmol $Sr(OH)_2$ were dissolved in 1.5 mL deionized water, and the pH was adjusted to be larger than 13 using 8 M KOH. The mixture were kept in oil bath at 100, 120, 140, 160 °C for 2, 5, 10, 30 min and inserted into the mixture of water and NaCl with temperature as low as -8 °C. Finally, the precipitate was collected after centrifuged and washed with deionized water and ethanol and dried at 50 °C for 24 h. It is noteworthy that the same stirring condition should be performed to maintain the diffusion rate caused by stirring.

2.3 Characterization

X-ray diffraction (XRD) was performed with a PANalytical X'pert diffractometer operated at 40 kV and 40 mA using Cu k_α radiation. Raman spectroscopy was performed on a Renishaw Ramascope 1000 with a green SpectraPhysics Argon laser with a wavelength of 524.5 nm. Transmission electron microscopy (TEM), high-resolution TEM (HRTEM) and selected area electron diffraction (SAED) images were recorded on a FEI Tecnai G2 20 microscopy operated at 200 kV. Scanning electron microscopy (SEM) and energy dispersive X-ray spectroscopy (EDXS) were carried out on an EVOMA 15 microscopy equipped with EDAX detector. Diffuse reflectance spectra (DRS) data were recorded on a Shimadzu UV-2600 spectrophotometer equipped with an integrating sphere using $BaSO_4$ as the reflectance standard sample. The nitrogen sorption isotherm and Brunauer-Emmett-Teller (BET) surface area were determined by nitrogen adsorption method (Quadrasorb SI), the sample was degassed at 150 °C for 4 h under vacuum atmosphere. X-ray photoelectron spectroscopy (XPS) measurements were measured on a Thermo ESCALAB 250Xi with Al Kα emission at 1486.6eV, and all of the binding energies were referenced to the C1s at 284.8eV.

2.4 Photoelectrochemical and photocatalytic activity tests

The PEC properties were studied by the CHI 660 electrochemical workstation in 0.5 M Na_2SO_4 solution, with a saturated calomel electrode (SCE) as the reference electrode, platinum wire as the counter electrode and fluorine-doped tin oxide (FTO) conducting glass covered with $SrTiO_3$ as the working electrode. The MVL-210 (MEJIRO GENOSSEN) visible light source was used as the light resource ($\lambda > 378$ nm). The $SrTiO_3$ films were coated by a doctor blading technique.

For photocatalytic hydrogen production test, 20 mg $SrTiO_3$ obtained from different precursors were dispersed in 10 mL mixed solution of ethanol/water (V/V = 1/1). Before illumination, the system was deoxygenated with Ar for 20 min. Under constant magnetic stirring, the system was exposed to the illumination of high pressure mercury lamp (Hanovia, 500 W, 100 $mW \cdot cm^{-2}$). The amount of hydrogen evolved was periodically detected by GC/TCD (Shimadzu, GC-14B) with a 5 Å molecular sieve column, using CH_4 as the internal standard. The two different $SrTiO_3$ samples were investigated under the same condition.

3 Results and discussion

3.1 Crystal structure

Fig. 1a shows the XRD patterns of the prepared TO-NS and commercial TO-NP. All of the diffraction peaks are consistent with anatase TiO_2 (tetragonal, $I4_1/amd$, lattice constants $\alpha = 3.785$ Å, $b = 3.785$ Å, $c = 9.514$ Å, JCPDS 21-1272). Nevertheless, the full width at half maximum (FWHM) of TO-NS and TO-NP exhibited different behaviors. The FWHM of both (101) and (200)

peaks for TO-NP is 0.544, whereas the corresponding FWHM for TO-NS is 0.420 and 0.305, respectively, revealing the anisotropic morphology of TO-NS. Moreover, although the Raman modes at 140, 390, 513 and 534 cm^{-1} of both TO-NS and TO-NP can be assigned as E_g, B_{1g}, A_{1g} (or B_{1g}), E_g modes of anatase TiO_2 (inset of Fig. 1a),[28] the intensity of TO-NS is relatively lower than that of TO-NP, which indicated the chemical adsorbed F^- on the surface of TO-NS influences the vibration modes of TiO_2.[28]

Hydrothermal treatment of anatase TiO_2 and $Sr(OH)_2$ in alkaline condition affords the formation of $SrTiO_3$. The dominated diffraction peaks of the products are identical to cubic $SrTiO_3$ (JCPDS 35-0734) (cf. Fig. 1b). In addition, the XRD patterns also reveal small traces of unreacted anatase TiO_2 and $Sr(OH)_2$. Especially, SrF_2 is found in the final products if using TO-NS as precursor, which on the other hand demonstrated F^- adsorbed on the surface of TO-NS, agreeing well with the observation from Raman spectra (inset of Fig. 1a). The diffraction peaks of $SrTiO_3$ prepared from TO-NS exhibited a slight shift to lower angle compared to that prepared from TO-NP. Hence, the unit cell parameters have been determined to be α = 3.904 (1) Å and α = 3.892 (2) Å, respectively.

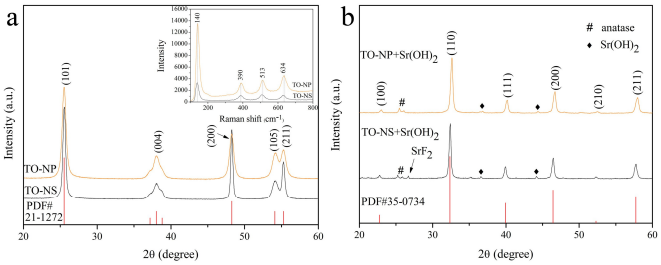

Fig. 1 a) XRD patterns of TO-NS and TO-NP precursors (inset: the corresponding Raman spectra); b) XRD patterns of the products prepared from TO-NP and TO-NS.

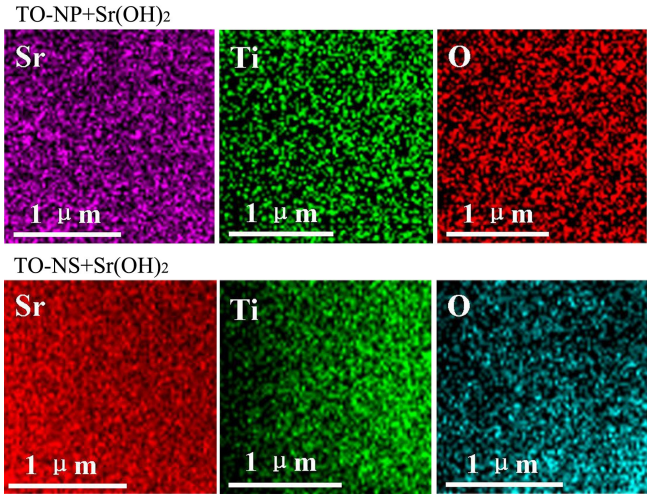

Fig. 2 EDXS mappings of $SrTiO_3$ prepared from different precursors

The EDXS investigations clearly demonstrate that the $SrTiO_3$ products displayed the same compositions that both contained Sr, Ti, O elements. Mapping of these three elements indicated that they have uniform distributions (Fig. 2). Fig. S1 shows the nitrogen-desorption curves of TiO_2 precursors and $SrTiO_3$ products. The corresponding parameters are listed in Table 1. After hydrothermal treatment, the BET surface area of $SrTiO_3$ products decreased no matter which precursors were used. Moreover, compared to the commercial TiO_2 nanoparticles, the synthesized TiO_2 nanosheets and their corresponding $SrTiO_3$ products showed a larger pore size.

Table 1 BET surface area and pore parameters of anatase TiO_2 precursors and $SrTiO_3$ products

	TO-NP	TO-NS	TO-NP +$Sr(OH)_2$	TO-NS +$Sr(OH)_2$
$S_{BET}/m^2 \cdot g^{-1}$	106.0	88.2	29.6	25.3
Pore Volume/$cc \cdot g^{-1}$	0.339	0.465	0.103	0.142
Pore Size/nm	12.7	20.7	14.1	22.2

3.2 Hydrothermal crystallization of $SrTiO_3$

To exclude the influences of cooling process of stainless steel autoclave on the reaction pathways, time-resolved quenching experiments have been performed through using Duran quartz glass tubes at 140 °C with reaction time of 2, 5, 10 and 30 min. Unexpectedly, the hydrothermal formation of $SrTiO_3$ is relatively fast. Perovskite-type $SrTiO_3$ phase has already been clearly observed only after 2 min of reaction no matter using TO-NP or TO-NS as a precursor (cf. Fig. 3), which is much faster than the hydrothermal crystallization of $BaTiO_3$ and $CaTiO_3$ with the requirement of hours of reaction time.[22, 23] Fig. S2 shows the schematic crystal structures of anatase TiO_2 and $SrTiO_3$. Both of them contain TiO_6 octahedra. Nevertheless, there are two kinds of Ti-O bonds in anatase TiO_2 with bond distances of 1.934Å and 1.980 Å, whereas $SrTiO_3$ only have one kind of Ti-O bond with distance of 1.952 Å. Sr atoms could occupy the gap among the TiO_6 octahedra to realize the transformation from tetragonal anatase TiO_2 to cubic $SrTiO_3$. According to Fig. 3, several diffraction peaks from SrF_2 were observed after 2 min of reaction if using TO-NS as precursor. These results confirmed the existence of Ti-F bonds on the surface of TO-NS. Under hydrothermal condition, Ti-F bonds on the surface could hydrolyze. Hence, F atoms are replaced by OH^- groups and F^- can be released.[26] Therefore, SrF_2 can be formed and depicted as

$$\equiv Ti\text{-}F + H_2O \rightarrow \equiv Ti\text{-}OH + H^+ + F^- \quad (1)$$

$$Sr^{2+} + 2F^- \rightarrow SrF_2 \quad (2)$$

Thus, the different transformation time could be attributed to the hydrolysis of Ti-F groups. Furthermore, on the basis of the analysis of the peak intensity of $SrTiO_3$, the hydrothermal crystallization of $SrTiO_3$ from anatase TiO_2 was almost finished in 30 min.

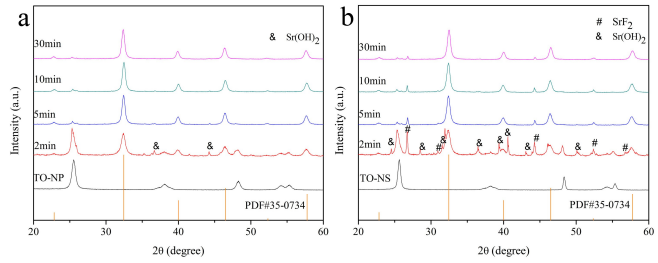

Fig. 3 Time-resolved XRD patterns recorded at 140 °C from different precursors: (a) TO-NP; (b) TO-NS

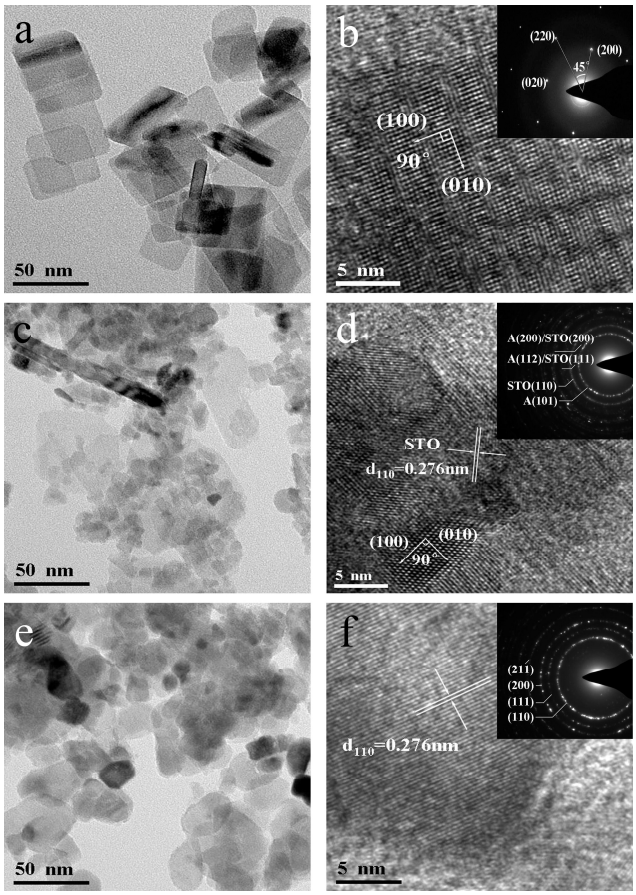

Fig. 4 (a) TEM image of the prepared TO-NS and (b) corresponding HRTEM image (inset: SAED pattern); (c) TEM image of the product prepared from TO-NS after 2 min of reaction time at 140 °C and (d) corresponding HRTEM image (inset: SAED pattern); (e) TEM image of the product prepared from TO-NS after 5 min of reaction time at 140 °C and (f) corresponding HRTEM image (inset: SAED pattern)

TEM, HRTEM as well as SAED were performed to investigate the morphological and microstructural evaluation of anatase TiO_2 precursor under hydrothermal condition. Fig. 4a shows the TEM image of TO-NS, which consists of uniform, well-defined sheet-like morphology with side length of 40 nm and thickness of 6 nm (Fig. S3) on the average. HRTEM images (Fig. 4b and Fig. S3) in combination with SAED (inset of Fig. 4b) revealed that the top and bottom planes of TO-NS are the {001} facets. Based on these results, it can be confirmed that the prepared TO-NS is anatase TiO_2 nanosheets with dominant {001} facets. After 2 min of reaction, it was observed that the products still contained sheet-liked morphology. However, some additional tiny particles with size of several nanometers were clearly observed (cf. Fig. 4c). According to the HRTEM image (Fig. 4d), the (001) surface of TO-NS can be maintained after hydrothermal treatment of 2 min, but an additional fringe spacing of 0.276 nm corresponding to the (110) atomic planes of $SrTiO_3$ was already observed, which is consistent with the results from XRD (Fig. 3b) and SAED (inset of Fig. 4d). Although {101} facets of anatase TiO_2 have a lower energy than that of {001} facets, {101} facets were not observed during the hydrothermal transformation process within the time resolution of our experiments. Prolong the reaction time to 5 min, the products were finally dominated by $SrTiO_3$ nanocrystals with particle size from 10 to 50 nm (Fig. 4e and f). On the whole, the morphology and crystal facets of TO-NS cannot be maintained during the hydrothermal transformation process, which differs from the previous reported topochemical reaction.[30]

To compare with the hydrothermal formation of $SrTiO_3$ from TO-NS with dominant {001} facets, Fig. 5 shows the TEM, HRTEM images and SAED patterns of TO-NP precursor and the products at different reaction time. TO-NP exhibited irregular morphology and the fringe spacing of 0.352 and 0.317 nm with an angle of 68° match well with the (101) and (003) planes of anatase TiO_2 (Fig. 4a and b), indicating that they have different morphology and crystal facets from TO-NS. Similar to the use of TO-NS as precursor, some tiny particles were already formed only after 2 min of reaction (Fig. 5c). Except the fringes spacing from anatase crystal structure of TiO_2, another set of the fringes spacing measures 0.276 nm, corresponding to the (110) lattice of $SrTiO_3$ (Fig. 5d). After 5 min of reaction, the products were dominated by $SrTiO_3$ nanocrystals, which have tendency to aggregate into larger agglomeration to reduce their surface energy (Fig. 5e). All in all, it can be concluded that the hydrothermal formation of $SrTiO_3$ under our reaction conditions is not based on the solid-solid transformation. Otherwise, these tiny nanoparticles should not be observed during the initial reaction process (cf. Fig. 4c and 5c). The formation process of $SrTiO_3$ could be similar to our previous work on the hydrothermal growth of $Bi_6S_2O_{15}$ nanowires using commercial Bi_2O_3 particles as starting materials.[31,32] At the early stage, the surface hydrolysis could occur to form hydroxytitanium complexes ($Ti(OH)_x^{4-x}$) under hydrothermal condition and subsequent slight dissolution of the starting anatase TiO_2 nanoparticles.[29] The difference for using TO-NS as precursor is that Ti-F bonds were also broken via hydrolytic attack except for Ti-O bonds. Then, the $Ti(OH)_x^{4-x}$ is capable of reaction with Sr ions to form $SrTiO_3$ nuclei at the solid/liquid interface, which appears to be a heterogeneous nucleation process. Therefore, the growth of $SrTiO_3$ is based on the expense of the dissolution of TiO_2 precursor. As perovskite $SrTiO_3$ has isotropic cubic crystal structure, no anisotropic morphology was observed for the hydrothermal products (Fig. 4e and 5e). Based on this formation mechanism, the rapid dissolution of TiO_2 precursor is crucial to provide the solution with a sufficient supply of titanium species. Thus, the particle size of TiO_2 precursor could have significantly influence on the hydrothermal formation rate of $SrTiO_3$. Fig. S4 compares the XRD patterns of the products using TiO_2 with bigger particle size

(TO-BP, several hundreds of nanometers) to the products obtained from TO-NS and TO-NP. After 10 min of reaction time, the ratio of $SrTiO_3$ in the products is much lower if using TO-BP as precursor, indicating a slower reaction rate. Moreover, the products were dominated by TiO_2 and $SrTiO_3$ particles with the size of hundreds of nanometers instead of nanocrystals (cf. Fig. S5).

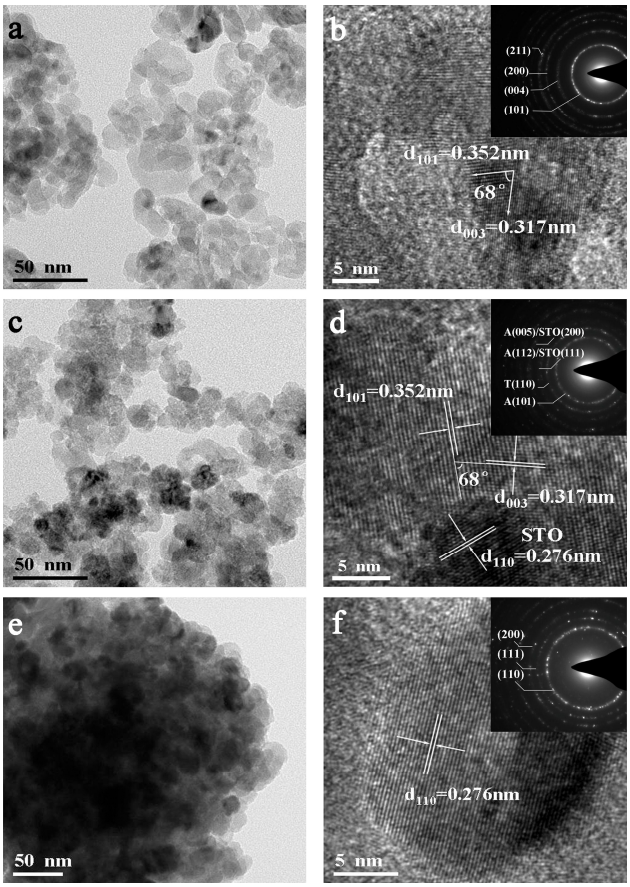

Fig. 5 (a) TEM image of the commercial TO-NP and (b) corresponding HRTEM image (inset: SAED pattern); (c) TEM image of the product prepared from TO-NP after 2 min of reaction time at 140 °C and (d) corresponding HRTEM image (inset: SAED pattern); (e) TEM image of the product prepared from TO-NP after 5 min of reaction time at 140 °C and (f) corresponding HRTEM image (inset: SAED pattern)

In order to further investigate the hydrothermal formation mechanism of $SrTiO_3$, the kinetics of the products from different precursors at 100, 120, 140 and 160 °C by the time-resolved quenching experiments were studied. Kinetic analyses are performed by fitting the data of the most intense reflection (110) of $SrTiO_3$ to the expression that correlate the extent of reaction α to time.[33-36] Fig. 6 shows the extent of reaction α of the $SrTiO_3$ (110) reflection as a function of temperature from different precursors. No induction time t_{ind} could be observed at all the investigated temperatures within the time resolution on the experimental setup, indicating that the formation of $SrTiO_3$ sets in immediately. As expected, the reaction was accelerated with increasing the reaction temperature which was reflected from the reduction of half-life time $t_{0.5}$ of $SrTiO_3$ formation: $t_{0.5}$ decreased from 5 to 1.2 min and 7.8 to 1.5 min for using TO-NP and TO-NS as precursors, respectively, when the temperature was raised from 100 to 160 °C (Table 2). In addition, the shape of the growth profile revealed the growth mechanism.[34] At lower temperature (100 and 120 °C), the $SrTiO_3$ growth curves exhibited distinctly difference for using TO-NP and TO-NS as precursors, indicating that they were dominated by different reaction mechanisms. These results revealed that Ti-F bonds on the surface of {001} facets of TO-NS could affect both the reaction rate and growth mechanisms. However, as the velocity of the $SrTiO_3$ formation is relatively fast (in 2 min), it is extremely difficult to perform Sharp-Hancock plots for a further evaluation of the obtained kinetic data giving the time resolution of the experiments.[37]

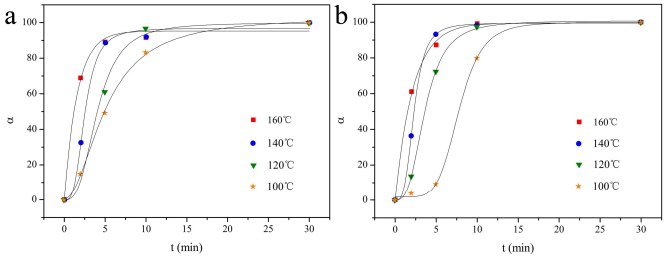

Fig. 6 Extent of reaction α versus time for the (110) reflection of $SrTiO_3$ recorded at different temperatures prepared from (a) TO-NP and (b) TO-NS.

Table 2 Summary of the t_{ind} and $t_{0.5}$ for the hydrothermal growth of $SrTiO_3$ under different reaction conditions within the time resolution on the experimental setup

T/°C	$t_{0.5}$ / *min*	$t_{0.5}$ / *min*
	TO-NP + $Sr(OH)_2$	TO-NS + $Sr(OH)_2$
100	5.0	7.8
120	3.9	3.6
140	2.5	2.2
160	1.2	1.5

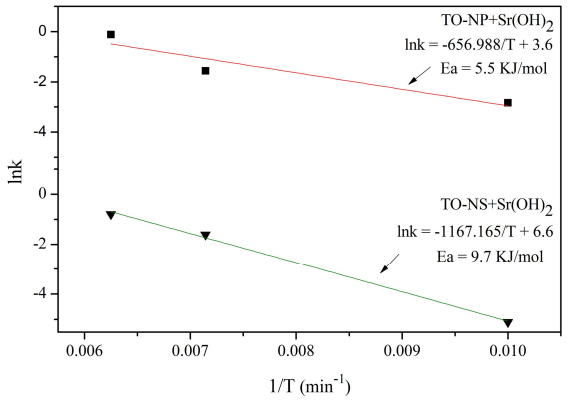

Fig. 7 Arrhenius plots for hydrothermal crystallization of $SrTiO_3$ from anatase TiO_2.

Moreover, the activation energy E_a for the hydrothermal crystallization of $SrTiO_3$ was calculated according to Arrhenius equation.[22] Fig. 7 shows the Arrhenius plots for the crystallization of $SrTiO_3$. The linearity of the plot demonstrated the feasibility to determine the E_a. The E_a determined by linear regression is 5.5

and 9.7 kJ mol^{-1} for using TO-NP and TN-NS as precursor, respectively. The E_a of TO-NS is larger than that of TO-NP. It could be attributed to the hydrolysis of Ti-F bond on the surface of TO-NS. Therefore, higher energy is needed for nucleation. Furthermore, the E_a of $SrTiO_3$ in our current work is much lower than the previous reported E_a of $BaTiO_3$ (21.0 kJ mol^{-1}).[22] Tsumura et al have previously demonstrated that $SrTiO_3$ is more easily formed than $BaTiO_3$ under the same reaction condition,[7] which is in line with our current E_a calculation. In addition, the nanoscale dimension of the precursor could be another reason (Fig. S4).

3.3 Optical properties and photocatalytic activities

The UV-vis absorption spectra of the $SrTiO_3$ products prepared from TO-NP and TO-NS precursors were showed in Fig. 8. The $SrTiO_3$ obtained from TO-NS exhibited a slight stronger absorption in the visible-light range compared to the products obtained from TO-NP. The band gap (E_g) of these two samples was determined to 3.26 and 3.37 eV, respectively, according to the onset of the absorption edge.

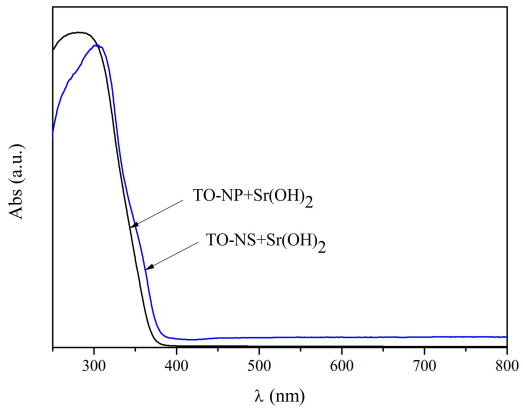

Fig. 8 UV-vis spectra of the $SrTiO_3$ products prepared from different TiO_2 precursors.

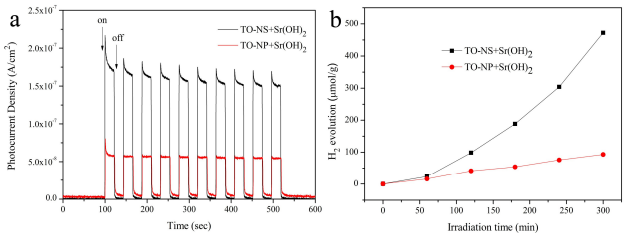

Fig. 9 (a) photocurrent versus time measurements of $SrTiO_3$ prepared from TO-NP and TO-NS precursors; (b) photocatalytic hydrogen production evolution of $SrTiO_3$ prepared from TO-NP and TO-NS precursors.

Fig. 9 shows the transient photocurrent responses for $SrTiO_3$ products obtained from different precursors. It is worth noting that the photocurrent of $SrTiO_3$ obtained from TO-NS is about three times higher than that of the products obtained from TO-NP. In accord with the photocurrent measurements, the $SrTiO_3$ obtained from TO-NS display a five times higher photocatalytic hydrogen evolution rates (95 μmol/h/g) compared to that of products obtained from TO-NP (19 μmol/h/g). All of these results clearly indicated that the crystal facets of TiO_2 precursors could not only affect the hydrothermal crystallization of $SrTiO_3$ but also have significantly influence on their properties and application performances. As the BET surface area (25.3 m^2/g) of $SrTiO_3$ obtained from TO-NS is even lower than that (29.6 m^2/g) from TO-NP, the enhanced H_2 production activity cannot be attributed to the surface area.

The electronic structures of $SrTiO_3$ products are further investigated by XPS. The characteristic peaks of Sr 3d, Ti 2p and O 1s for both $SrTiO_3$ keep almost unchanged (Fig. 10a, 10b and 10c). Fig. 10d shows the valence band XPS spectra of $SrTiO_3$ products. The VB maximum of $SrTiO_3$ prepared from TO-NS is 1.95 eV, which is 0.07 eV lower than that prepared from TO-NP. Considering the 0.09 eV difference of the band gap (Fig. 8), these two $SrTiO_3$ products have very similar CB minimum which is around -1.33 eV. The Mott-Schottky (MS) measurements were performed and Fig. 11 shows the MS plots of the $SrTiO_3$ products. The flat band potential, V_{fb}, calculated from the x intercepts of the linear region, was -1.15 *vs.* SCE for $SrTiO_3$ obtained from TO-NS, whereas $SrTiO_3$ prepared from TO-NP was -1.14 *vs.* SCE. All of these results confirmed that both $SrTiO_3$ products have very closed CB minimum, which is large enough to reduce H^+ to H_2 (0 eV *vs.* NHE). Therefore, H_2 production under light irradiation was observed for both samples. F 1s XPS spectra of $SrTiO_3$ products obtained from TO-NS indicated the existence of F^- in the final products (Figure S6). Combining with the BET surface area measurements and band structure investigations, F^- adsorbed on the surface of {001} facets of TiO_2 could not only influence the hydrothermal crystallization of $SrTiO_3$, but also affect their performances. Nevertheless, as SrF_2 byproduct was observed from XRD (Fig. 1b), it is difficult to identify the F^- doping in $SrTiO_3$, which needs further investigations.

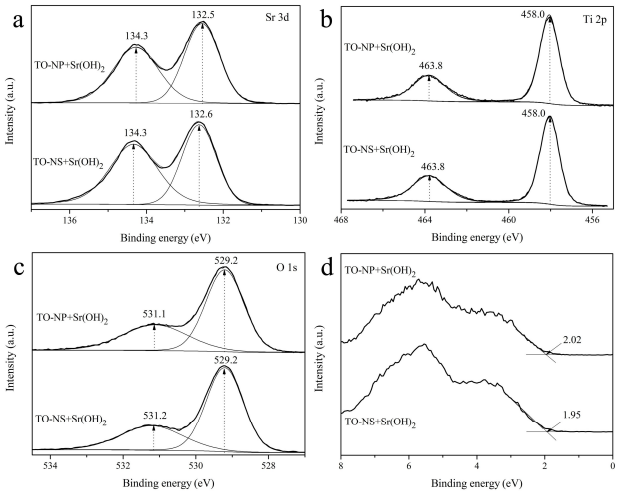

Fig. 10 (a) Sr 3d, (b) Ti 2p and (c) O 1s XPS spectra of $SrTiO_3$ synthesized from different TiO_2 precursors, (d) valence band XPS spectra of $SrTiO_3$ products

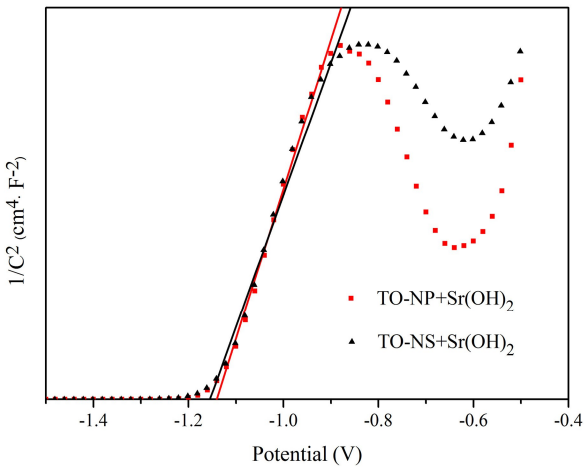

Fig. 11 Mott-Schottky (MS) plots of $SrTiO_3$ products

4. Conclusion

In summary, we compared the hydrothermal crystallization of $SrTiO_3$ using anatase TiO_2 nanosheets with dominant {001} facets and commercial anatase TiO_2 nanoparticles as precursors by time resolved quenching experiments. The velocity of hydrothermal formation of $SrTiO_3$ was relatively fast and the crystallization process of $SrTiO_3$ had almost finished in 30 min in the given interval. As surface adsorbed F^- is indispensable to stabilize the {001} facets of anatase TiO_2, SrF_2 was observed during the whole reaction process if using TiO_2 with {001} facets as precursor, which could slow down the reaction rate. Nevertheless, no matter which kind of anatase TiO_2 precursors were used, the initial particle morphology and exposed crystal facets of TiO_2 precursor cannot be retained in the final $SrTiO_3$ products. Thus, a two-step sequence has been proposed for the hydrothermal formation of $SrTiO_3$ starting from a minute of dissolution of the solid TiO_2 precursor, followed by $SrTiO_3$ nucleation and growth at the solid/liquid interface. Moreover, the $SrTiO_3$ obtained from TO-NS exhibited a three times higher photocurrent and five times higher photocatalytic hydrogen evolution rates compared to the $SrTiO_3$ prepared from TO-NP.

Acknowledgements

This work was financially supported by the Large Scientific Apparatus Joint Funds of the National Natural Science Foundation of China (U1232119), the Innovative Research Team of Sichuan Provincial Education Department and SWPU (2012XJZT002) and Sichuan Provincial College Students' Innovation and Entrepreneurship Training Plan (S14014).

Notes and references

[a] *State Key Laboratory of Oil and Gas Reservoir Geology and Exploitation, Southwest Petroleum University, Xindu Rd. 8, Chengdu 610500, China. Fax: +86 2883 037406; Tel: +86 2883 037411; E-mail: yzhou@swpu.edu.cn*

[b] *School of Materials Science and Engineering, Southwest Petroleum University, Xindu Rd. 8, Chengdu 610500, China*

[c] *School of Chemistry and Chemical Engineering, Southwest Petroleum University, Xindu Rd. 8, Chengdu 610500, China*

† Electronic Supplementary Information (ESI) available: [nitrogen adesorption-desorption curves; schematic crystal structures of anatase TiO_2 and $SrTiO_3$; the cross section HRTEM image of TO-NS precursor; the XRD patterns of the products after 10 min of quenching experiments at 140 °C prepared from different anatase TiO_2 precursors; SEM images of TiO_2 particles with bigger size and the corresponding products; F 1s XPS spectra]. See DOI: 10.1039/b000000x/

1 T. Hara, T. Ishiguro, N. Wakiya and K. Shinozaki, *Mater. Sci. Eng. A*, 2009, **161**, 142-145.
2 M. Miyauchi, M. Takashio and H. Tobimatsu, *Langmuir*, 2004, **20**, 232-236.
3 J. Hanzig, M. Zschornak, M. Nentwich, F. Hanzig, S. Gemming, T. Leisegang and D. C. Meyer, *J. Power Sources*, 2014, **267**, 700-705.
4 S. M. Yang, H. Z. Kou, J. C. Wang, H. B. Xue and H. L. Han, *J. Phys. Chem. C*, 2010, **114**, 4245-4249.
5 G. R. Patzke, Y. Zhou, R. Kontic, and F. Conrad, *Angew. Chem. Int. Ed.*, 2011, **50**, 826-859.
6 S. C. Zhang, J. X. Liu, Y. X. Han, B. C. Chen and X. G. Li, *Mater. Sci. Eng. B*, 2004, **110**, 11-17.
7 T. Tsumura, K. Matsuoka and M. Toyoda, *J. Mater. Sci. Technol.*, 2010, **26**, 33-38.
8 Y. F. Zhang, G. Xu, X. Wei, Z. H. Ren, Y. Liu, G. Shen and G. R. Han, *CrystEngComm*, 2012, **14**,3702-3707.
9 G. Xu, S. Q. Deng, Y. F. Zhang, X. Wei, X. Yang, Y. Liu, G. Shen, and G. R. Han, *CrystEngComm*, 2014, **16**, 2025-2031.
10 G. Xu, Z. H. Tao, Y. G. Zhao, Y. F. Zhang, Z. H. Ren, G. Shen, G. R. Han and X. Wei, *CrystEngComm*, 2013, **15**, 1439-1444.
11 N. Park, Y. F. Wang, W. S. Seo, F. Dang, C. L. Wan and K. Koumoto, *CrystEngComm*, 2013, **15**, 679-685.
12 X. Wei, G. Xu, Z. H. Ren, C. X. Xu, W. J. Weng, G. Shen and G. R. Han, *J. Am. Ceram. Soc.*, 2010, **93**, 1297-1305.
13 K. Katagiri, Y. Miyoshi and K. Lnumaru, *J. Colloid. Interface. Sci.*, 2013, **407**, 282-286.
14 H. W. Bai, J. Juay, Z. Y. Liu, X. X. Song, S. S. Lee and D. D. Sun, *Appl. Catal. B*, 2012, **125**, 367-374.
15 T. P. Cao, Y. J. Li, C. H. Wang, C. L. Shao and Y. C. Liu, *Langmuir*, 2011, **27**, 2946-2952.
16 Y. J. Li, T. P. Cao, C. H. Wang, C. L. Shao, *Chem. J. Chinese. U.*, 2011, **32**, 2490-2497.
17 X. M. Zhang, K. F. Huo, L. S. Hu, Z. W. Wu and P. K. Chu, *J. Am. Ceram. Soc.*, 2010, **93**, 2771-2778.
18 L. M. Guo, X. H. Wang, H. Zhang and L. T. Li, *Ceram. Int.*, 2013, **39**, S633-S636.
19 J. Zhang, J. H. Bang, C. C. Tang and P.V. Kamat, *ACS nano*, 2010, **4**, 387-395.
20 O. Ruzimuradov, S. Nurmanov, M. Hojamberdiev, R. M. Prasad, A. Gurlo, J. Broetz, K. Nakanishi and R. Riedel, *Mater. Lett.* , 2014, **116**, 353-355.
21 Q. Kuang and S. H. Yang, *ACS. Appl. Mater. Inter.*, 2013, **5**, 3683-3690.
22 R. I. Walton, F. Millange, R. I. Smith, T. C. Hansen and O'Hare, *J. Am. Chem. Soc.*, 2001, **123**, 12547-12555.
23 D. Croker, M. Loan and B. K. Hodnett, *Cryst. Growth Des.*, 2009, **9**, 2207-2213.
24 T. R. N. Kutty, R. Vivekanandan and P. Murugaraj, *Mater. Chem. Phys.*, 1988, **19**, 533-546.
25 H. G. Yang, C. H. Sun, S. Z. Qiao, J. Zou, G. Liu, S. C. Smith, H. M. Cheng and G. Q. Lu, *Nature*, 2008, **453**, 638-641.
26 X. H. Yang, Z. Li, C. H. Sun, H. G. Yang and C. Z. Li, *Chem. Mater.*, 2011, **23**, 3486-3494.
27 X. G. Han, Q. Kuang, M. S. Jin, Z. X. Xie and L. S. Zheng, *J. Am. Chem. Soc.*, 2009, **131**, 3152-3153.
28 H. F. Wang, L. Y. Chen, W. N. Su, J. C. Chung and B. J. Hwang, *J. Phys. Chem. C*, 2010, **114**, 3185-3189.
29 J. O. Eckert Jr, C. C. Hung-Houston, B. L. Gerstan, M. M. Lenka and E. R. Riman, *J. Am. Ceram. Soc.*, 1996, **79**, 2929-2939.

30 T. X. Wang, S. Z. Liu and J. Chen, *Powder Technol.*, 2011, **205**, 289-291.
31 Y. Zhou, J.-D. Grunwaldt, F. Krumeich, K. B. Zheng, G. R. Chen, J. Stötzel, R. Frahm and G. R. Patzke, *Small*, 2010, **6**, 1173-1179.
32 Y. Zhou, G. R. Patzke, *CrystEngComm*, 2012, **14**, 1161-1163.
33 Y. Zhou, E. Antonova, W. Bensch and G. R. Patzke, *Nanoscale*, 2010, **2**, 2412-2417.
34 Y. Zhou, E. Antonova, Y. H. Lin, J. D. Grunwaldt, W. Bensch and G. R. Patake, *Eur. J. Inorg. Chem.*, 2012, 783-789.
35 Y. Zhou, N. Pienack, W. Bensch and G. R. Patzke, *Small*, 2009, **5**, 1978-1983.
36 Y. Zhou, Q. Zhang, Y. H. Lin, E. Antonova, W. Bensch and G. R. Patzke, *Sci. China Chem.*, 2013, **56**, 435-442.
37 A. Michailovski, J.-D. Grunwaldt, A. Baiker, R. Kiebach, W. Bensch and G. R. Patzke, *Angew. Chem. Int. Ed.*, 2005, **44**, 5643-5647.